ACADEMIC PRESS

Available online at www.sciencedirect.com

SCIENCE DIRECT®

Journal of Magnetic Resonance 161 (2003) 258–264

JMR Journal of Magnetic Resonance

www.elsevier.com/locate/jmr

Communication

Symmetrical reconversion: measuring cross-correlation rates with enhanced accuracy

Philippe Pelupessy,[a] Guillermo Minguez Espallargas,[b] and Geoffrey Bodenhausen[a,*]

[a] *Département de Chimie, associé au CNRS, Ecole Normale Supérieure, 24 rue Lhomond, Paris Cedex 05 F-75231, France*
[b] *University of Seville, Facultad de Quimica, c/o Profesor García González, s/n, Sevilla 41012, Spain*

Received 21 October 2002; revised 13 December 2002

Abstract

A new strategy has been developed to measure cross-correlation rates with much enhanced accuracy. The method relies on the use of four complementary experiments. Errors due to pulse miscalibration and to uncontrolled attenuation factors associated with relaxation are cancelled out. Problems due to violations of the secular approximation are greatly alleviated. The method has been applied to the measurement of N/NH (CSA/DD) cross-correlated relaxation rates in human ubiquitin.

Keywords: Cross-correlation rates; Chemical shift anisotropy; Dipole–dipole interaction

Cross-correlated relaxation rates can provide valuable information on structure [1–4], internal dynamics [5–8], and chemical shift anisotropy (CSA) tensors [8–11]. Two distinct approaches can be used to determine cross-correlation rates. In the frequency-domain approach, the rates can be directly extracted from the peak heights of different lines in a multiplet, which are inversely proportional to their widths. These lines correspond to different operators in a single transition basis, which relax with different rates under the influence of cross-correlated relaxation [12]. In a Cartesian product operator basis on the other hand, cross-correlation can be described in terms of an interconversion of different terms in the density operator. This can be exploited in the time-domain approach, where the rates are obtained by measuring the decay of an initial operator P and the build-up of a target operator Q that is created by cross-correlated relaxation. The ratio between the expectation values of the two operators is given by [5]

$$\frac{\langle Q\rangle(t)}{\langle P\rangle(t)} = \tanh(R_{CC}t), \tag{1}$$

where R_{CC} is the cross-correlation rate, which can thus be obtained directly either by measuring the intensities of the two operators at a single time $t = T$, or from a so-called "build-up curve" as a function of t. The time-domain method allows one to record highly resolved spectra that are not encumbered by multiplets, and the method is usually more sensitive than the frequency-domain approach [13]. Moreover, the time-domain method is also applicable to the measurement of longitudinal cross-correlation rates [14] and to cases where the scalar couplings are smaller than the line-widths.

In Fig. 1a, the principle that has been used hitherto for most time-domain experiments is outlined. In a first step an initial operator P is excited. In the subsequent relaxation period T, cross-relaxation leads to a partial transformation of the initial density operator P into the target operator Q, while coherent evolution under shifts and couplings is refocused. At the end of the interval T, there has been a partial decay of P and a build-up of Q. Two complementary experiments are then performed. In experiment A (using the nomenclature of Tjandra et al. [5]), one detects $\langle Q\rangle(T)$, while $\langle P\rangle(T)$ is observed in experiment B. In order to detect the expectation value $\langle Q\rangle(T)$, the operator Q is converted into P during the conversion period M^A, using suitable transformations under scalar couplings and radio frequency (RF) pulses,

* Corresponding author. Fax: +33-1-44-32-33-97.
E-mail address: Geoffrey.Bodenhausen@ens.fr (G. Bodenhausen).

1090-7807/03/$ - see front matter © 2003 Elsevier Science (USA). All rights reserved.
doi:10.1016/S1090-7807(02)00190-8

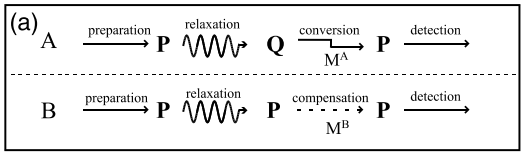

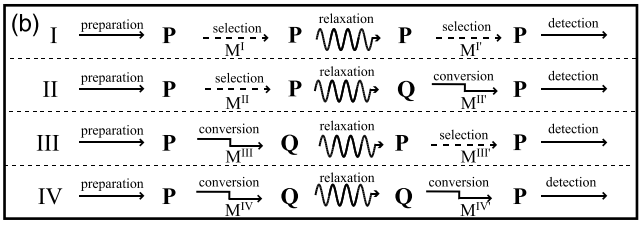

Fig. 1. Schemes for the measurement of a cross-correlation rate R_{CC} that leads to the inter-conversion of two operators P and Q. (a) In the traditional approach the conversion of P into Q (i.e., the build-up of Q) is detected in experiment A, while the decay of operator P is measured in experiment B. In experiment A the operator Q is converted into P by coherent evolution in the conversion interval M^A before detection, while in experiment B an extra compensation interval M^B is usually inserted to achieve an approximate compensation for relaxation losses during M^A. (b) In the novel symmetrical reconversion approach, a set of four experiments is used: (I) and (IV) to monitor the decay of the operators P and Q and (II) and (III) to monitor the conversion from P into Q and vice-versa. Special care needs to be taken to select the appropriate operators before and after the relaxation intervals. The losses that occur during the different conversion and selection intervals precisely cancel out.

a process that is of course attenuated by relaxation and pulse errors. Usually an extra compensation interval M^B is inserted in experiment B so that the signals are attenuated in a similar fashion in experiments A and B. The conversion, compensation and detection blocks can sometimes be contracted into shorter sequences.

Two problems may arise with this conventional scheme, which has been used in a wide variety of cross-correlation experiments in recent years. First, systematic errors may arise if the auto-relaxation rates of the operators P and Q during the relaxation period T are different, since this leads to deviations from Eq. (1) [15–17]. Second, it may be difficult to assess the extent of losses due to relaxation and pulse errors during the conversion period M^A. In Liouville space, where the elements of the density operator σ expressed in the Cartesian product operator base are written as a vector, the efficiency of the conversion can be written as a product with a non-unitary matrix

$$\sigma_f = M^A \sigma_i, \tag{2}$$

where σ_i and σ_f are the initial and final states of the density operator before and after the conversion period M^A in experiment A. Using a combination of phase-cycling and pulsed field gradients, it is usually possible to start with a pure operator $\sigma_i = Q$ at the beginning of the conversion interval M^A, and one can selectively observe an operator $\sigma_f = P$ at the end of this interval, so that only one element of the matrix M^A affects the outcome of the experiments

$$\langle P \rangle = M^A_{PQ} \langle Q \rangle, \tag{3}$$

where M^A_{PQ} is the element of the matrix M^A that describes the partial conversion of the operator Q into P (note the antichronological order of the indices). In principle, one could calculate such an element, but this requires precise knowledge of a variety of transverse and longitudinal relaxation rates, scalar couplings and pulse imperfections. Often it is more convenient to insert an extra compensation interval M^B in experiment B, without coherent evolution, designed so that relaxation losses are very similar to those occurring in the conversion interval M^A of experiment A.

To achieve a more satisfying compensation of systematic errors, we propose to replace the conventional pair of experiments {A, B} by a set of four experiments {I–IV} as shown in Fig. 1b. This scheme will be referred to as "symmetrical reconversion." Experiment I is closely related to experiment B of the previous scheme. However, in contrast to the interval M^B discussed above, the transformations M^I_{PP} and $M^{I'}_{PP}$ do *not* correspond to delays that are long enough for relaxation to play a role, but only to a selection of the operator P immediately before and after the relaxation period T. These selection processes can be represented by matrices M^I and $M^{I'}$. Experiment II is almost identical to experiment A in the conventional scheme, except that special care is taken to select the operator P before the relaxation period T (transformation M^{II}_{PP}, which is identical to M^I_{PP}) and to convert the operator Q into P after T (non-unitary transformations $M^{II'}_{PQ}$, which is comparable to M^A_{PQ} in the conventional experiment). Experiment III is very similar to experiment II, except that the conversion from P into Q happens *before* the relaxation time T, a process which is described by a non-unitary transformation M^{III}_{QP} that is related by symmetry to $M^{II'}_{PQ}$. In this case the "reverse" build-up of the operator P starting with Q is measured in the interval T. Of course, $M^{III'}_{PP}$ and $M^{I'}_{PP}$ are again identical. Finally, experiment IV, which allows one to measure the auto-relaxation of the operator Q in the T interval, uses both conversion periods that are employed in experiments II and III, represented by M^{IV}_{QP} that is identical to M^{III}_{QP} and by $M^{IV'}_{PQ}$ that is identical to $M^{II'}_{PQ}$. Thus the losses during the selection and conversion periods can be accounted for by real attenuation factors that need not be determined experimentally nor evaluated by simulation. In analogy to Eq. (1)

$$\frac{\langle P \rangle_{II}(t)}{\langle P \rangle_{I}(t)} = \frac{M^{II}_{PP} M^{II'}_{PQ}}{M^{I}_{PP} M^{I'}_{PP}} \tanh(R_{CC} t) = \frac{M^{I}_{PP} M^{II'}_{PQ}}{M^{I}_{PP} M^{I'}_{PP}} \tanh(R_{CC} t) \tag{4a}$$

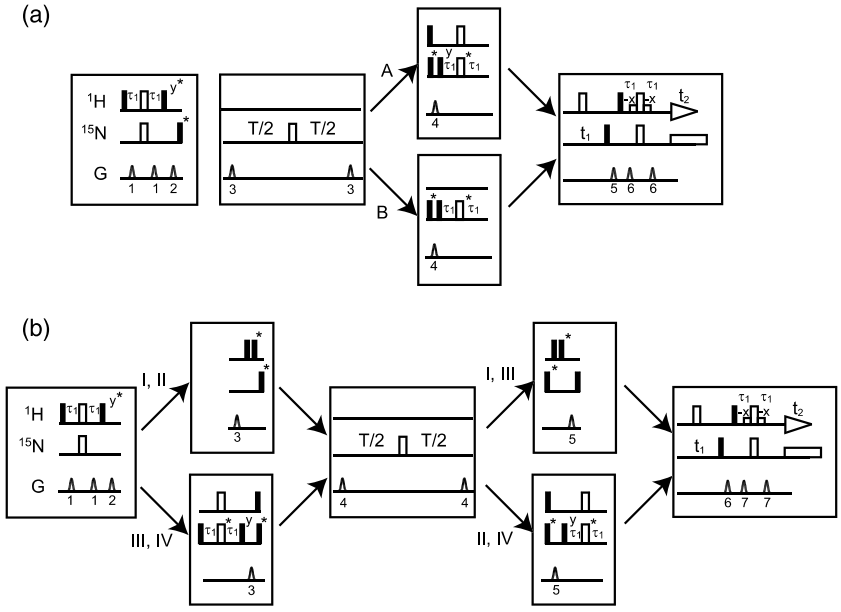

Fig. 2. (a) Conventional experiments for the measurement of N/NH^N (CSA/DD) cross-correlation rates as proposed by Schwalbe [4], divided into four blocks according to the scheme of Fig. 1a. (b) Improved version of these experiments according to the symmetrical conversion scheme of Fig. 1b. Filled and open rectangles correspond to $\pi/2$ and π pulses. The wider open rectangles correspond to selective $\pi/2$ pulses applied to the H_2O resonance. All phases are along the x-axis, unless indicated otherwise. The $\pi/2$ pulses marked by asterisks are phase-alternated independently while the signals are added and subtracted. The π pulses marked by an asterisk are switched independently between the x- and y-axes while changing the receiver sign.

and

$$\frac{\langle P\rangle_{\mathrm{III}}(t)}{\langle P\rangle_{\mathrm{IV}}(t)} = \frac{M_{QP}^{\mathrm{III}} M_{PP}^{\mathrm{III}'}}{M_{QP}^{\mathrm{IV}} M_{PQ}^{\mathrm{IV}'}} \tanh(R_{\mathrm{CC}}t) = \frac{M_{QP}^{\mathrm{III}} M_{PP}^{\mathrm{I}'}}{M_{QP}^{\mathrm{III}} M_{PQ}^{\mathrm{II}'}} \tanh(R_{\mathrm{CC}}t). \tag{4b}$$

Hence

$$\sqrt{\frac{\langle P\rangle_{\mathrm{II}}(t)}{\langle P\rangle_{\mathrm{I}}(t)} \frac{\langle P\rangle_{\mathrm{III}}(t)}{\langle P\rangle_{\mathrm{IV}}(t)}} = |\tanh(R_{\mathrm{CC}}t)|. \tag{5}$$

Using Eq. (5) one can obtain the rate R_{CC} independently of the efficiency of the various selection and conversion periods. The information about the sign of the rate is lost, but this can easily be recovered by looking at the signs of the intensities in the individual experiments. Since one starts once with the operator Q and once with the operator P, problems due to differences in auto-relaxation rates of these two operators during the relaxation period T will also be alleviated (see simulations below).

The new symmetrical reconversion method can readily be adapted to measure various CSA/DD and DD/DD cross-correlation rates. Note that some experiments, in particular those designed to measure CSA/CSA cross-correlation rates, require two complementary experiments that only differ in the phases of some of the RF-pulses, so that they do not suffer from asymmetric reconversion.

It is useful to compare stochastic errors due to thermal noise in the conventional and in the new symmetrical schemes. Let us assume that the losses in the conversion periods before and after the relaxation interval T are the same, i.e., $M_{PQ}^{\mathrm{II}'} \approx M_{QP}^{\mathrm{III}} = \alpha$. The signal intensity in experiment I is normalised to 1. The fraction of the coherence that is transformed by cross-correlated relaxation is defined to be β. Thus the relative intensities of experiments I, II, III, and IV are equal to 1, $\alpha\beta$, $\alpha\beta$, and α^2. The intensities in the conventional experiments A and B, also normalised to experiment I, will be $2\alpha\beta$ and 2α (the factors 2 arise because one has twice as much time for each experiment). Let σ be the stochastic errors in experiments I–IV divided by the signal intensity in experiment I. The stochastic errors in experiments A and B, if they are also divided by the signal intensity in experiment I, will be $\sqrt{2}\sigma$. Error propagation for the ratio of Eq. (1) leads to

$$E_{\mathrm{AB}} = \frac{\sigma}{\alpha\sqrt{2}}\sqrt{1+\beta^2}, \tag{6}$$

while for the ratio in Eq. (5) one obtains errors

$$E_{\mathrm{I–IV}} = \frac{\sigma}{\alpha\sqrt{2}}\sqrt{1+\beta^2(\alpha^2+\alpha^{-2})/2}. \tag{7}$$

One can see that the errors are identical for an ideal conversion ($\alpha = 1$), but they increase in the new scheme when $\alpha < 1$. The difference will only be appreciable when $\alpha < \beta$. The new approach does not depend on the specific details of the conversion blocks, hence one can easily optimise the efficiency α of the conversion to minimise stochastic errors.

In order to demonstrate the utility of the new method, we shall have a closer look at an experiment designed by Tjandra et al. [5] to measure N/NH (CSA/DD) cross-correlation rates in proteins. In Fig. 2a the conventional experiments A and B proposed by Tjandra et al. are drawn following the pattern of Fig. 1a. Fig. 2b shows how the experiments can be adapted according to the principles of symmetrical reconversion to give four sequences I–IV. In the conventional sequence of Fig. 2a the operator $2N_yH_z$ is initially created by an INEPT transfer step combined with three pulsed field gradients. Experiments I and II of Fig. 2b follow the same procedure, except that the final $\pi/2$ pulse of INEPT is delayed until after two $\pi/2$ proton pulses with phases $(+x, +x)$ or $(+x, -x)$, which amounts to an alternation between π and $0°$ pulses. This ensures that only the anti-phase component ($P = 2N_yH_z$) is retained at the beginning of the interval T. In experiments III and IV the final $\pi/2$ nitrogen pulse is again removed from the initial INEPT sequence, and this is followed by a second INEPT-like sequence which leads to an in-phase component ($P = N_y$) at the beginning of T. A proton $\pi/2$ pulse and a pulsed field gradient destroy any residual anti-phase terms $2N_xH_z$ or $2N_yH_z$ at this point. All six schemes of Fig. 2 use a nitrogen π pulse in the middle of the relaxation interval T to refocus coherent evolution. In the conventional experiment A of Fig. 2a, the interval T is followed by nitrogen and proton $\pi/2$ pulses and by a gradient pulse, so that only the build-up of the in-phase term $Q = N_y$ is detected. This term is converted into an anti-phase term $2N_yH_z$ by a subsequent INEPT-like step. In experiment B the decay of the anti-phase operator $P = 2N_yH_z$ is detected. In order to account for the relaxation losses that occur in experiment A, a compensation interval M^B of duration $2\tau_1$ is inserted in B, but without any proton pulses. In both new experiments I and III, the operator $P = 2N_yH_z$ needs to be selected after the interval T. In order to avoid contamination with the in-phase term N_y, two proton $\pi/2$ pulses (the second of which is alternated in phase in concert with the receiver phase) are inserted immediately after the nitrogen $\pi/2$ pulse. The remaining anti-phase operator $2N_yH_z$ is then converted back into observable magnetization. In experiments II and IV the in-phase component N_y is transformed into an antiphase operator $2N_yH_z$. This occurs in a manner identical to experiment A. All six schemes of Fig. 2 have identical t_1 evolution intervals where the nitrogen coherence evolves and t_2 detection periods where the amide proton magnetization is observed, in the manner of heteronuclear single-quantum correlation spectrosocpy (HSQC).

In Fig. 3a simulations are presented in order to evaluate the validity of Eqs. (1) and (5) as a function of the relaxation time T. A scalar coupling ${}^1J_{NH} = -93\,Hz$, a cross-correlation rate $R_{N,NH} = 4\,s^{-1}$ and a longitudinal proton relaxation rate $R_{1H} = 5\,s^{-1}$ have been assumed,

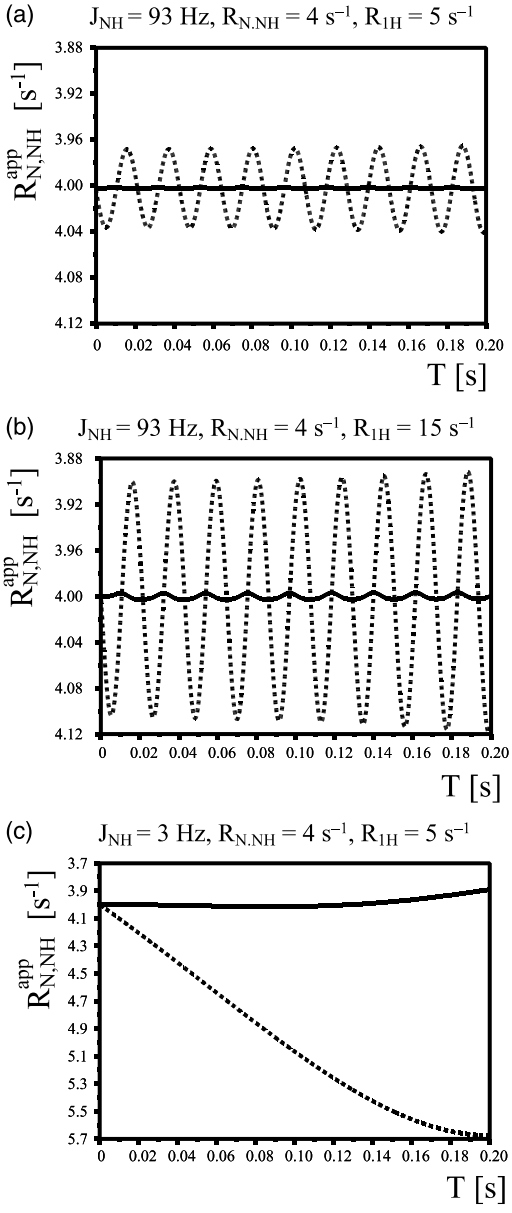

Fig. 3. Numerical simulations to verify the validity of Eqs. (1) and (5). The dashed lines correspond to simulations of the conventional experiments of Fig. 2a, where the apparent cross-correlation rate $R^{app}_{N,NH}$ has been obtained using Eq. (1). The bold lines correspond to the symmetrical conversion scheme of Fig. 2b, where $R^{app}_{N,NH}$ has been obtained with Eq. (5). In (a) parameters have been used that are typical for an amide NH system in a protein with a correlation time of 4 ns, a proton Lamor frequency of 600 MHz and a temperature of 300 K ($J_{NH} = -93\,Hz$, $R_{N,NH} = 4\,s^{-1}$, $R_{1H} = 5\,s^{-1}$). In (b), the longitudinal proton relaxation rate was increased to $R_{1H} = 15\,s^{-1}$ to account for faster chemical exchange or for a longer correlation time (larger protein), all other parameters being the same. In (c), the scalar coupling was decreased to $J_{NH} = 3\,Hz$ to simulate long-range correlations, all other parameters being as in (a). In all three cases, the relative errors of $R^{app}_{N,NH}$ do not depend on the rate $R_{N,NH}$ (simulations not shown).

as would be expected for a small protein with an isotropic rotational correlation time $\tau_c = 4\,ns$. Using these parameters for a two-spin system the evolution of the Liouvillian has been calculated numerically for the

relaxation periods T of Figs. 2a and b. In the simulations the effects of the nitrogen auto-relaxation rates cancel out, although in experiments they would lead to a reduced signal-to-noise ratio. The apparent relaxation rates $R^{app}_{N,NH}$ that are obtained from Eqs. (1) and (5) are plotted for different values of T. In the conventional scheme (dashed lines) deviations as large as 1% can be seen. In the new scheme (continuous lines) the deviations from Eq. (5) are smaller than 0.01%. When the longitudinal proton relaxation rate R_{1H} is increased to $15\,s^{-1}$ (Fig. 3b) the maximum deviations increase to 3% and 0.1% for the conventional and for the new schemes. A judicious choice of the relaxation time T can reduce errors in the original scheme [17], however it is difficult to account for scalar couplings that are unknown and often not uniform. In the new scheme the relaxation delay T can be chosen at will. The advantages become far more dramatic when the scalar coupling is very small, which occurs for long-distance cross-correlation effects such as $C'/C'H^N$ (CSA/DD), where one must expect a violation of the secular approximation. Simulations like those of Fig. 3a are shown in Fig. 3c, except that the scalar coupling was reduced to 3 Hz. With the new scheme, the systematic errors remain below 0.5% even for relaxation times T as long as 0.14 s, whereas the conventional scheme leads to errors of more than 30%.

We have applied the new symmetrical sequences to a sample of ^{15}N labelled human ubiquitin with relaxation delays $T = 40$, 80 (twice) and 120 ms. In Figs. 4a–c the rates obtained with Eq. (5) for different T are compared with the average over all four experiments. (These averages are our best estimates and may be regarded as the "true" values of the rates.) The rates obtained for different relaxation delays T agree remarkably well with each other. We have also used the conventional sequence of Tjandra et al. [5] with approximately the same parameters as in the original publication with a relaxation delay $T = 46.7$ ms. As can be seen in Fig. 4d, there is a systematic deviation of about 4% in this case. There may be several causes for these deviations. First, the deviation from Eq. (1) is expected to be nearly at its worst for $T = 46.7$ ms. Second, there are differences between the relaxation rates of the relevant operators in the intervals M^A and M^B of experiments A and B. Not only does one have to account for differential relaxation of longitudinal terms (N_z compared to $2N_zH_z$), but during M^A the relaxation rate is the average between those of N_y and $2N_xH_z$, while in M^B it is close to the relaxation rate of $2N_yH_z$. The difference between these relaxation

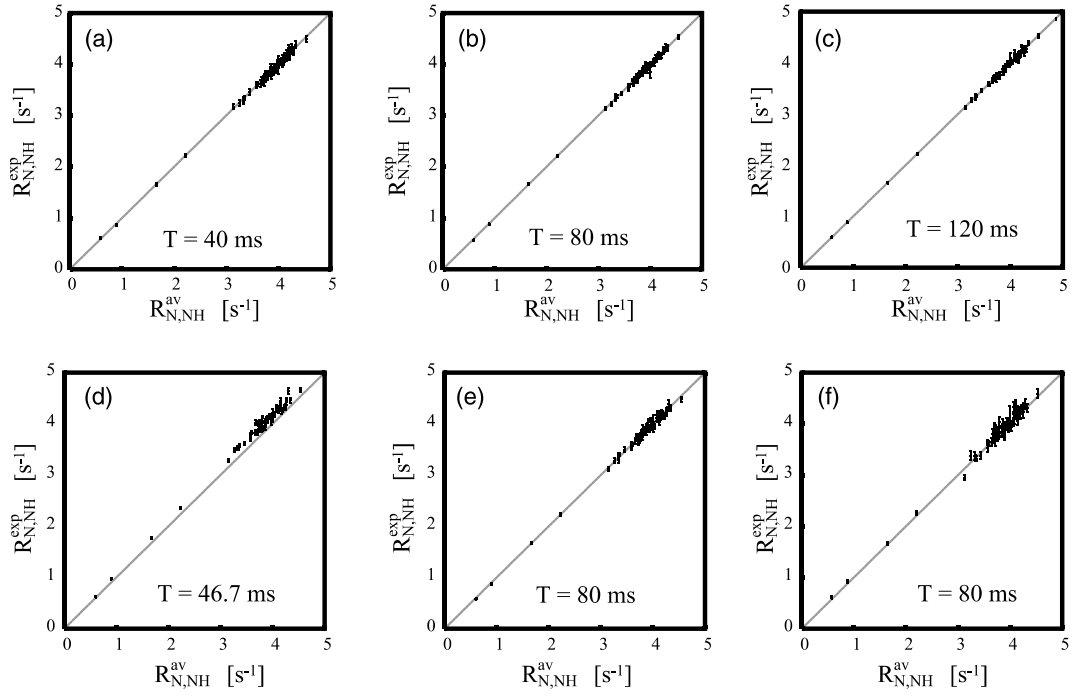

Fig. 4. (Top row) Experimental rates obtained with the symmetrical reconversion sequences of Fig. 2b applied to a sample of ^{15}N-labelled human ubiquitin at 300 K and a proton Larmor frequency of 600 MHz. (a)–(c) Experiments performed with relaxation delays $T = 40$, 80 and 120 ms (a fourth experiment was performed with $T = 80$ ms). The experimental cross-correlation rates $R^{app}_{N,NH}$ obtained using Eq. (5) for various residues are plotted against the rates averaged over all four measurements. A number of 32 scans per t_1 increment were taken in each of the four experiments (I–IV), resulting in a total experimental time of 13 hours for each delay T. (d) Conventional experiments (A, B) of Fig. 2a recorded under the same conditions as in (a)–(c) with a relaxation delay $T = 46.7$ ms and 64 scans per t_1 increment for each experiment A and B, plotted against the same average rates used along the abcissae in the top row. (e) Same as (b) but with shorter delays $2\tau_1 = 3$ ms instead of 5.3 ms in the conversion blocks. (f) Same as (b) but with all proton pulses shortened by 20%. Experiments I–IV and A–B have been recorded in an interleaved manner for each T value.

rates is, to a good approximation, given by the longitudinal proton relaxation rate R_{1H}. With a rate $R_{1H} = 5\,s^{-1}$ this can lead to a deviation of more than 1% in the ratio between the two intensities. A third source of error lies in the preparation part of the conventional experiments A and B: a long gradient has been applied between the first INEPT step and the relaxation period T. During this period longitudinal cross-correlated relaxation takes place. For a protein with a rotational correlation time of 4 ns at 600 MHz this rate is about 20% of the transverse relaxation rate. The resulting error depends on the duration of the gradient and subsequent recovery period and on the relaxation time T. In the experiment of Fig. 4d the duration of the gradient and recovery period was about 5 ms, which leads to a deviation of about 2% for $T = 46.7$ ms. All of these effects lead to an increase of the apparent rates. By contrast, two other factors may lead to an decrease of the apparent rates. Proton pulse imperfections lead to an incomplete inversion of the protons in scheme A, unless composite pulses were used. Furthermore, cross-correlated relaxation has different effects during the conversion and compensation periods in schemes A and B. In scheme A the cross-correlation rate is averaged out by the proton π pulse, while in scheme B it is not. The resulting asymmetry will be exacerbated by the fact that no care has been taken to select the anti-phase operator after the relaxation period T so that the in-phase operator might contribute to the signal intensities (especially for longer relaxation times T). The original sequence could be improved by introducing the two selection blocks with two nitrogen pulses as in the new scheme I. Also the relaxation time T could be chosen in such a way that the averaging of the in- and anti-phase relaxation rates occurs over both relaxation and conversion periods. However this might be difficult to achieve when the J couplings are not uniform. Extra pulses might introduce additional errors due to their imperfections. In the new scheme errors due to pulse imperfections will simply cancel out.

In order to test the robustness of the scheme we have repeated the experiment at 80 ms but with delays $2\tau_1 = 3$ ms instead of 5.3 ms during the conversion blocks. A delay of $2\tau_1 = 3$ ms corresponds to an optimum for a scalar coupling of 167 Hz instead of 93 Hz. The transfer efficiency drops by a factor of about 0.7. As can be seen from Fig. 4e this does not lead to any systematic deviations of the apparent rates. The precision of the rates, as reflected in the standard deviation, has decreased somewhat because of signal losses during the conversion periods. In another experiment we deliberately miss-calibrated all proton pulses by 20% (using 9 μs instead of 11.0 μs for $\pi/2$ pulses, and 18 μs instead of 22.0 μs for π pulses). The systematic errors remain small (Fig. 4f) although stochastic errors increase considerably due to a significant degradation of the signal-to-noise ratio. Note that the suppression of anti-phase terms by proton pulses that deviate from $\pi/2$ is not perfect, so that the conditions of symmetrical reconversion are not properly fulfilled in this case, but even with such large calibration errors the systematic errors remain small. With normal precautions to calibrate the pulse widths or by using composite $\pi/2$ pulses, the systematic errors can be safely neglected.

In conclusion, we have developed a new principle for the measurement of cross-correlation rates with enhanced accuracy. The method relies on four complementary experiments designed so that the ratios of signal intensities are largely independent of experimental parameters. Problems due to violations of the secular approximation are greatly alleviated. The sensitivity is similar to conventional approaches.

Acknowledgments

We are indebted to Dr. Sapna Ravindranathan and Dr. Jens Dittmer for helpful comments. This work was supported by the European Union through the Research Training Network "Cross-Correlation" HPRN-CT-2000-00092.

References

[1] J. Boyd, U. Hommel, V.V. Krishnan, Influence of cross-correlation between dipolar and chemical shift anisotropy relaxation mechanisms upon the transverse relaxation rates of ^{15}N in macromolecules, Chem. Phys. Lett. 187 (1991) 317–324.

[2] B. Reif, M. Hennig, C. Griesinger, Direct measurement of angles between bond vectors in high-resolution NMR, Science 276 (1997) 1230–1233.

[3] K. Kloiber, W. Schuler, R. Konrat, Automated NMR determination of protein backbone dihedral angles from cross-correlated spin relaxation, J. Biomol. NMR 22 (2002) 349–363.

[4] H. Schwalbe, Cross-correlated relaxation for measurement of angles between tensorial interactions, Methods Enzymol. A 338 (2001) 35–81.

[5] N. Tjandra, A. Szabo, A. Bax, Protein backbone dynamics and ^{15}N chemical shift anisotropy from quantitative measurement of relaxation interference effects, J. Am. Chem. Soc. 118 (1996) 6986–6991.

[6] B. Brutscher, N.R. Skrynnikov, T. Bremi, R. Bruschweiler, R.R. Ernst, Quantitative investigation of dipole-CSA cross-correlated relaxation by ZQ/DQ spectroscopy, J. Magn. Reson. 130 (1998) 346–351.

[7] V.A. Daragan, K.H. Mayo, Motional model analyses of protein and peptide dynamics using ^{13}C and ^{15}N NMR relaxation, Prog. Nucl. Magn. Reson. Spectrosc. 31 (1997) 63–105.

[8] D. Frueh, Internal motions in proteins and interference effects in nuclear magnetic resonance, Prog. Nucl. Magn. Reson. Spectrosc. 41 (2002) 305–324.

[9] R. Ghose, K. Huang, J.H. Prestegard, Measurement of cross correlation between dipolar coupling and chemical shift anisotropy in the spin relaxation of ^{13}C, ^{15}N-Labeled proteins, J. Magn. Reson. 135 (1998) 487–499.

[10] Y.X. Pang, E.R.P. Zuiderweg, Determination of protein backbone (CO)-^{13}C chemical shift anisotropy tensors in solution, J. Am. Chem. Soc. 122 (2000) 4841–4842.
[11] D. Fushman, N. Tjandra, D. Cowburn, Direct measurement of ^{15}N chemical shift anisotropy in solution, J. Am. Chem. Soc. 120 (1998) 10947–10952.
[12] M. Goldman, Interference effects in the relaxation of a pair of unlike spin-1/2, J. Magn. Reson. 60 (1984) 437–452.
[13] T. Carlomagno, C. Griesinger, Errors in the measurement of cross-correlated relaxation rates and how to avoid them, J. Magn. Reson. 144 (2000) 280–287.
[14] C.D. Kroenke, J.P. Loria, L.K. Lee, M. Rance, A.G. Palmer III, Longitudinal and transverse ^{1}H-^{15}N dipolar/^{15}N chemical shift anisotropy relaxation interference: unambiguous determination of rotational diffusion tensors and chemical exchange effects in biological macromolecules, J. Am. Chem. Soc. 120 (1998) 7905–7915.
[15] A.G. Palmer III, N.J. Skelton, W.J. Chazin, P.E. Wright, M. Rance, Suppression of the effects of cross-correlation between dipolar and anisotropic chemical shift relaxation mechanisms in the measurements of spin–spin relaxation rates, Molec. Phys. 75 (1992) 699–711.
[16] T. Meersmann, G. Bodenhausen, Relaxation-induced oscillations of spin-echo envelopes, Chem. Phys. Lett. 257 (1996) 374–380.
[17] R. Ghose, J.H. Prestegard, Improved estimation of CSA-dipolar coupling cross-correlation rates from laboratory frame relaxation experiments, J. Magn. Reson. 134 (1998) 308–314.